A non-linear model of a rotary pneumatic servo system

N D Tillett[1], **N D Vaughan**[2] and **A Bowyer**[2]
[1]Bio-Engineering Division, Silsoe Research Institute, Bedford
[2]Fluid Power Centre, University of Bath

Abstract: A simulation model of a rotary pneumatic servo system has been developed and verified against an experimental system. The double-acting rotary actuator is a novel device utilizing flexible inflatable bladders. The device differs from conventional pneumatic cylinders in that it exhibits low levels of friction, as it has no sliding seals, but it does suffer from hysteresis caused by bladder distortion. The objective of this study was to develop a tool with which to investigate the effect of various forms of hysteresis and other parameters on system performance. The dynamic model utilizes a linearized analysis of pneumatic components based on earlier studies. The principal advance described in this paper relates to the inclusion of non-linear elements. These are hysteresis caused by friction or the distortion of flexible components, and a digital controller implementation. The simulation successfully predicted all major modes of behaviour. Simplified models of rubber and coulomb friction-induced hysteresis modified simulation performance in line with experimental results. An investigation in simulation showed that coulomb friction-induced hysteresis had a greater damping effect than that caused by distorting the bladders. This result applies only to position control, as hysteresis has been shown not to provide damping in trajectory control applications.

Keywords: pneumatic, simulation, control, hysteresis

NOTATION

C_1, C_2	valve coefficients
K_e	proportional to error gain
K_p	proportional to differential pressure gain
K_{tp}	proportional to transient pressure
K_v	proportional to velocity gain
M	mass flow
P_a, P_b	pressure in bladders
P_q	quiescent pressure
R	gas constant
T_s	air supply temperature
U_{out}	output voltage to valve
V_a, V_b	volume of bladders
X	valve spool displacement
α	first moment of area
γ	ratio of specific heats
θ_d	demand angle
θ_o	output angle
τ	system time constant
τ_f	high-pass filter time constant

Subscripts

i	initial value
a, b	clockwise and anticlockwise bladders

Lower case denotes a change from initial conditions.

The MS was received on 15 August 1996 and was accepted for publication on 30 January 1997.

1 INTRODUCTION

Pneumatic servo positioning systems offer the potential to provide robust, low-cost drives with high power–weight ratios. Furthermore, they can readily be made hygienic and washable for food applications. Traditionally their use has been limited to simple end-stop applications because of the difficulty of providing proportional control of position. This difficulty stems from the non-linear nature of air as a power transmission medium and non-linearities associated with pneumatic components. A number of researchers have devised non-linear control strategies to improve performance. Typical of these is work by Pu and Weston (**1**) who used null-value compensation to allow for friction-induced dead band, as well as using gain scheduling techniques to improve system stiffness without adversely affecting stability. Belforte *et al.* (**2**) applied fuzzy logic techniques and Surgenor *et al.* (**3**) investigated continuous sliding mode control. As a result of advances such as these, servo

pneumatic positioning systems are becoming commercially available. Most of these employ rodless cylinders which exhibit high levels of friction in their sliding seals.

In researching the application of robotics to the horticultural and food industries the authors have developed a novel rotary proportional pneumatic joint (**4**), which uses flexible inflatable elements (trade name 'Flexator') to provide motion. A feature of this joint is that there is virtually no sliding motion and therefore no inherent friction. A change in shape of the inflatable bladders, on the other hand, does introduce hysteresis through internal distortion of the rubber-backed woven material from which the bladder is constructed. The nature of the hysteresis caused by the distortion of this material and that caused by sliding friction is different.

In order to provide a tool for future investigation of the effect of various design parameters, notably hysteresis, on system performance a simulation model has been constructed. Model parameters match those of an existing experimental system which allowed validation to take place. The dynamic characteristics of the rotary pneumatic joint are very similar to those of conventional pneumatic cylinders and so it has been possible to base this work on earlier studies. The literature contains two approaches to pneumatic system modelling. In one followed by Backé and Eschmann (**5**), the system is broken down into a series of components which are modelled as a sequence of alternate resistances and capacities. The mass flowrate between components is calculated from pressures and temperatures and from parameters describing resistance, e.g. conductance and the critical pressure ratio which are measured experimentally. The advantage of this approach, which yields good results, is its ability to model characteristics such as those associated with choked flow. Frictional non-linearities have also been incorporated into this model. The other approach, followed by Lui and Bobrow (**6**), utilizes a linearized analysis of the pneumatic components and was based on earlier studies by Shearer (**7**). Their results, which do not take frictional effects into account, show reasonable agreement between experiment and simulation, but the match is not as good as that achieved by Backé and Eschmann (**5**). In this study, the latter approach using a linearized analysis of the pneumatic components has been chosen for its relative simplicity. However, non-linearities due to the distortion of the inflatable bladders have been incorporated into the model.

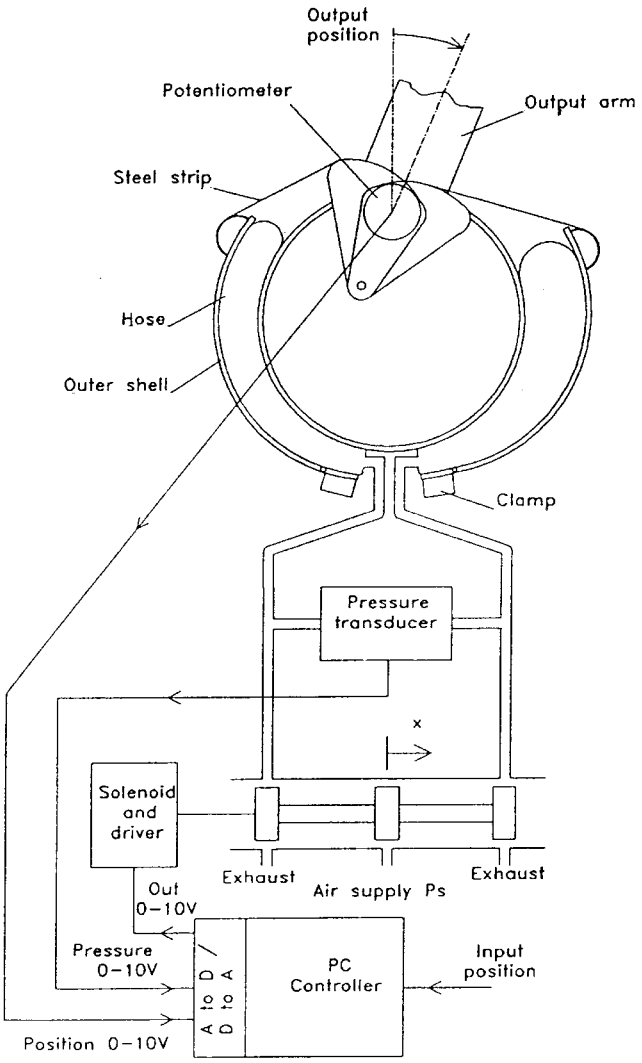

Fig. 1 Schematic of experimental system

2 ANALYSIS

2.1 Experimental system

A diagrammatic representation of the experimental system, which is described more fully in reference (**4**), is given in Fig. 1. Air is apportioned by a flow control valve into two flexible inflatable bladders wrapped around a 150 mm diameter aluminium tube. Each bladder consists of a length of lay flat fire hose folded back on itself and clamped to form a closed volume. Aluminium shells hinged at the clamped end of the hose cover the bladder and are connected to cams within the tube by a thin steel strip. As one bladder inflates relative to the other, the shell moves out, tensioning the steel strip, thereby causing the cam to rotate. The output arm is connected to the cams, thus providing a simple lightweight direct drive. Cam profiles are chosen to compensate for the reduction in tension in the steel strips that occurs with bladder inflation. A caliper brake with nylon pads acts on an aluminium disc which is directly connected to the output shaft. Braking force is controlled by varying the compression of a spring acting on the calipers.

The five-port proportional solenoid spool valve is an open-loop device in which spool position is proportional to solenoid current, the force from which is balanced by a coil spring. In order to minimize the effect of spool friction on spool position and therefore flowrate, a 50 Hz dither signal is superimposed on the control signal. The result is a

relatively robust low-cost valve, though its open-loop nature does result in some drift in neutral values and the dither signal, whose amplitude is 30 per cent of the full control range, does introduce feedback signal sampling difficulties.

Output position is measured by a plastic film potentiometer connected directly to the cam shaft. Differential pressure between the two bladders is measured with a piezoresistive device. Both transducers have been arranged to provide 0–10 V outputs over their working range. The control algorithm runs on a 386 PC in a 2.5 ms hardware interrupt loop. This is interfaced with the transducers and solenoid spool valve drivers through a proprietary 12 bit input/output card.

The control equation used for these experiments can be represented as follows:

$$U_{\text{out}} = K_{\text{e}}(\theta_{\text{o}} - \theta_{\text{d}}) - K_{\text{p}}(P_{\text{a}} - P_{\text{b}}) - K_{\text{v}}\dot{\theta}_{\text{o}} \tag{1}$$

where U_{out} is controller output voltage, K_{e}, K_{p} and K_{v} are controller gains, θ_{o} and θ_{d} are output and demand angles respectively and $P_{\text{a}} - P_{\text{b}}$ is the differential pressure between bladders.

2.2 Linearized servo system

The objective of this analysis is to derive linearized differential equations for the components of the system so that they can be presented in a transfer function (TF) form suitable for inclusion in a Simulink model. It has been shown by Shearer (**7**) using continuity and energy equations that for one chamber of a pneumatic cylinder (or one bladder of the flexible rotary actuator) mass flow M can be expressed as

$$\dot{m}_{\text{a}} = \frac{P_{\text{ai}}\dot{v}_{\text{a}}}{RT_{\text{s}}} + \frac{V_{\text{ai}}\dot{p}_{\text{a}}}{\gamma RT_{\text{s}}} \tag{2}$$

where P is the pressure and V is the volume of the chamber, R is the gas constant and T_{s} is the supply temperature, γ is the ratio of specific heats and lower case denotes a change from initial conditions where the subscript i indicates an initial value. Assumptions made in this derivation include perfect gas, adiabatic change and compressible flow. Similarly, the equation for the other side can be represented as

$$\dot{m}_{\text{b}} = \frac{P_{\text{bi}}\dot{v}_{\text{b}}}{RT_{\text{s}}} + \frac{V_{\text{bi}}\dot{p}_{\text{b}}}{\gamma RT_{\text{s}}} \tag{3}$$

Shearer (**7**) also proposed the following linearized pressure-flow characteristic representation for a pneumatic spool value:

$$\dot{m}_{\text{a}} = C_1 x - C_2 p_{\text{a}} \tag{4}$$

$$\dot{m}_{\text{b}} = -C_1 x - C_2 p_{\text{b}} \tag{5}$$

where X is spool displacement and

$$C_1 = \left.\frac{\delta\dot{M}_{\text{a}}}{\delta X}\right|_{P_{\text{ai}}} = \left.\frac{\delta\dot{M}_{\text{b}}}{\delta X}\right|_{P_{\text{bi}}} \tag{6}$$

$$C_2 = \left.\frac{\delta\dot{M}_{\text{a}}}{\delta P_{\text{a}}}\right|_{X_{\text{i}}} = \left.\frac{\delta\dot{M}_{\text{b}}}{\delta P_{\text{b}}}\right|_{X_{\text{i}}} \tag{7}$$

These relationships were also used by Burrows (**8**) to obtain the characteristic equation of a pneumatic servo system and to show the effect of cylinder position on stability. A similar manipulation of these equations is performed here in order to obtain a relationship between spool position and actuator pressures P_{a} and P_{b}.

Considering the volume of each bladder:

$$V_{\text{ai}} = V + \theta_{\text{i}}\alpha \tag{8}$$

$$V_{\text{bi}} = V - \theta_{\text{i}}\alpha \tag{9}$$

where V is the volume in either bladder at mid-stroke, θ_{i} is the actuator initial output angle and α is the first moment of area. Following a displacement θ from the initial conditions:

$$v_{\text{a}} = \theta\alpha \tag{10}$$

$$v_{\text{b}} = -\theta\alpha \tag{11}$$

Combining equation (2) with equation (4) and equation (3) with equation (5) and substituting equations (8), (9), (10) and (11),

$$C_1 x - C_2 p_{\text{a}} = \frac{P_{\text{ai}}\alpha\dot{\theta}}{RT_{\text{s}}} + \frac{(V + \alpha\theta_{\text{i}})\dot{p}_{\text{a}}}{\gamma RT_{\text{s}}} \tag{12}$$

$$-C_1 x - C_2 p_{\text{b}} = \frac{-P_{\text{bi}}\alpha\dot{\theta}}{RT_{\text{s}}} + \frac{(V - \alpha\theta_{\text{i}})\dot{p}_{\text{b}}}{\gamma RT_{\text{s}}} \tag{13}$$

Combining equations (12) and (13), rearranging and converting from dot to Laplace notation where s represents $\text{d}/\text{d}t$,

$$\frac{\alpha s\theta}{RT_{\text{s}}}\left[(P_{\text{ai}} + P_{\text{bi}}) + \frac{\theta_{\text{i}}}{\gamma RT_{\text{s}}}(P_{\text{ai}} - P_{\text{bi}})\right] = C_1 x - \left[C_2 + \frac{Vs}{\gamma RT_{\text{s}}} + \frac{(\alpha\theta_i/\gamma RT_{\text{s}})^2 s^2}{C_2 + V/\gamma RT_{\text{s}}}\right](P_{\text{a}} - P_{\text{b}}) \tag{14}$$

Initial pressure conditions are assumed to the same in each bladder:

$$P_{\text{ai}} = P_{\text{bi}} = P_{\text{q}}$$

where P_q is the quiescent pressure. Equation (14) can then be rearranged to give

$$\frac{2\alpha s\theta P_q}{RT_s} = 2C_1 x - G(s)(P_a - P_b) \tag{15}$$

where

$$G(s) = C_2\left\{\frac{[1-(\alpha\theta_i/V)^2]\tau^2 s^2 + 2\tau s + 1}{1+\tau s}\right\} \tag{16}$$

and the time constant

$$\tau = \frac{V}{\gamma R T_s C_2} \tag{17}$$

Thus an expression has been derived for $P_a - P_b$ in terms of x and $s\theta$, which is the result needed to construct the block diagram model in Section 3.

2.3 Analysis and measurement of system parameters

Linearized valve coefficients, C_1 and C_2, were evaluated experimentally by measuring flow at a range of differential pressures and spool positions. The large-amplitude pressure ripple caused by spool dither prevented the use of conventional flowmeters, particularly for low flows. Accordingly flows were deduced from the rate of charge of pressure vessels. The values used in the simulation of $C_1 = 1.5/\mathrm{kg\,m}$ and $C_2 = 0.4\mathrm{e}^{-8}$ ms were taken in the lower range of flowrates as this best represents the system when settling about a set point.

Hysteresis within the rubber-backed woven material bladders is thought to be due to relative motion between reinforcing fibres and the rubber matrix as the bladder distorts. The bladders change shape for two reasons, firstly due to changes in actuator output position and secondly due to changes in inflation pressure. The characteristics and parameters of both have been investigated experimentally. In one experiment an actuator output arm was connected to a strain gauge load cell which was in turn mounted on a lead screw actuated carriage to facilitate actuator movement over a limited stroke. Pressure in both bladders was held constant but unequal so that a nominally constant output torque could be maintained. The actuator was then cycled through part of its stroke while torque and position were logged. The results illustrated in Fig. 2a show ± 1.5 N m hysteresis which is ± 2 per cent of maximum output torque. This has been modelled as having a modified trapezoidal characteristic as depicted in Fig. 2b. For constant input pressures, output torque changes due to actuator movement vary first stepwise and then linearly with angular position up to the hysteresis boundary. Once beyond the hysteresis boundary it becomes saturated and the output force remains constant. Work by Chou and Hannaford (**9**) with an alternative form of inflatable reinforced rubber actuator (McKibben type) indicated that hysteresis characteristics were independent of velocity over a wide speed range. Within the limited speed capacity of the apparatus (0.01 rad/s) these results were confirmed and so hysteresis has been modelled as independent of speed.

In a second experiment the output position was fixed and the pressure in one bladder was varied, while that in the other remained constant. The resulting plot of torque versus pressure given in Fig. 2c indicates a hysteresis of ± 0.15 N m (± 0.2 per cent), a figure that remains fairly constant when the experiment is repeated at other operating pressures. It is likely that a proportion of this hysteresis was due to very small (0.25°, in the results illustrated) movements within the apparatus. Hysteresis due to variations in inflation pressure have been shown to be small in comparison to those due to changes in output position and have therefore not been included in the model.

Two types of friction were considered to be of possible significance: coulomb and stiction. Coulomb friction is considered as a constant torque which opposes motion; when there is no motion it opposes (but does not exceed) the applied force, as depicted in Fig. 2d. Stiction is regarded as a force which generally exceeds coulomb friction at speeds below a threshold. It too opposes motion and when there is no motion opposes (but does not exceed) the applied force. Tests using a tension testing machine indicated that a pure coulomb friction model adequately represents the caliper brake system.

3 SIMULATION

3.1 Model construction

The dynamic model was constructed within the SIMULINK/MATLAB program (**10**). This environment is well suited to a block diagram representation of the system, an outline of which is illustrated in Fig. 3.

The digital controller block is made up of a subsystem which includes analogue-to-digital and digital-to-analogue conversions, as well as the control algorithm itself. The control algorithm was written in the MATLAB language and called as an S-function m-file. MATLAB code is very similar to the C-code used in the experimental controller so that in most cases the code and its structure could be copied directly, thus minimizing the risk of differences between the experimental and model controllers.

The solenoid subsystem is a very simple combination of offset, gain and saturation blocks to convert the controller output voltage linearly to a spool displacement. No account has been taken of solenoid and spool dynamics as these are considered very fast in comparison with the actuator itself. Spool friction and valve null-value drift have also been neglected. A sine wave has been superimposed on the solenoid input to model valve dither. The valve subsystem consists of a block diagram representation of the transfer function derived in Section 2.2.

The actuator hysteresis block consists of two subsystems

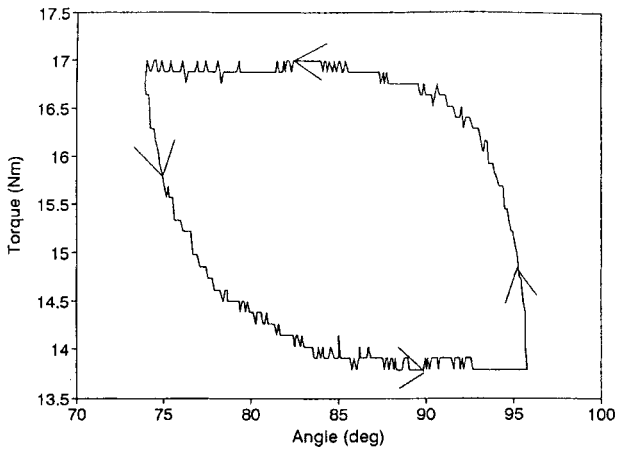

(a) Measured hysteresis due to movement of output arm with no brake applied, $P_a = 2.1$ bar, $P_b = 2.7$ bar

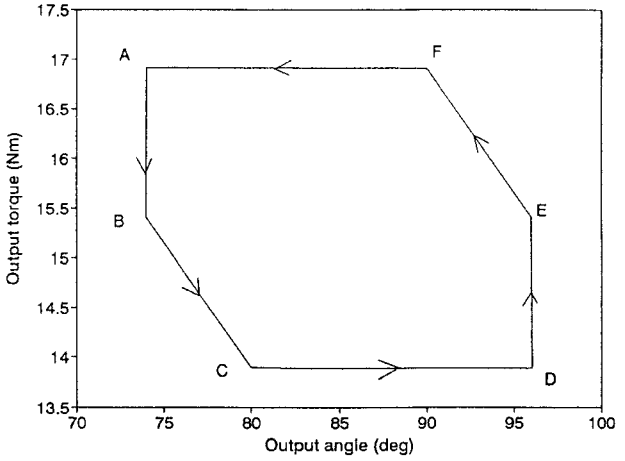

(b) Model of bladder distortion-induced hysteresis due to movement of output arm, $P_a = 2.1$ bar, $P_b = 2.7$ bar

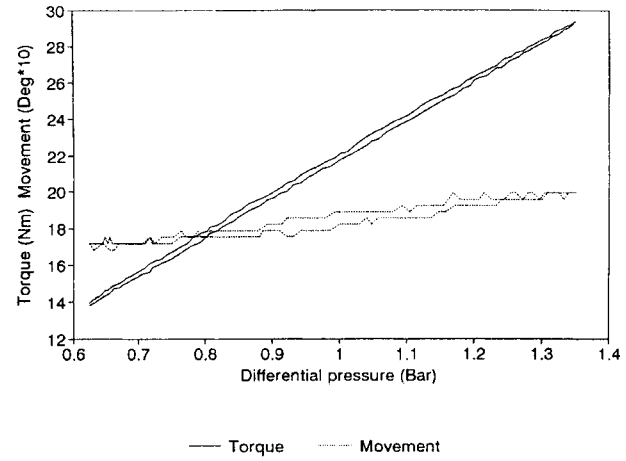

(c) Measured hysteresis due to changes in pressure ($P_a - P_b$) with no brake applied and output arm clamped

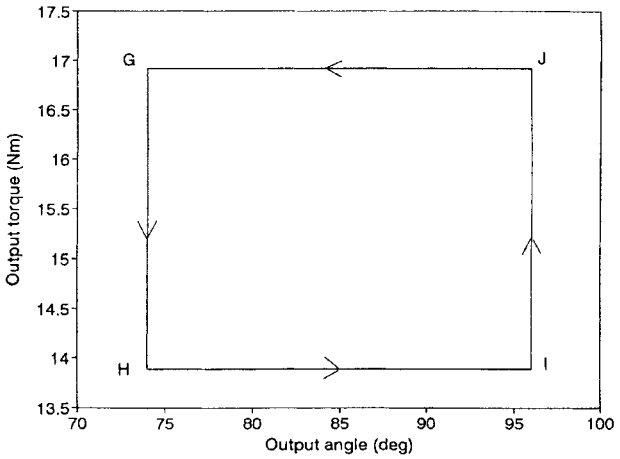

(d) Model of Coulomb friction-induced hysteresis due to movement of output arm

Fig. 2 Measured and idealized hysteresis in the output torque characteristic

acting in series (Fig. 3b). The first models that element of hysteresis which varies linearly with output position (i.e. B–C and E–F in Fig. 2b). The construction of this block is broken down in more detail in Fig. 3c. The second models hysteresis, which results in a stepwise change with the polarity of output motion (A–B and D–E in Fig. 2b and G–H and I–J in Fig. 2d). Both utilize MATLAB function m-files taking angle and torque as inputs. In the former, memory blocks are used to record the recent history of movement and in the latter a derivative block calculates angular velocity. These provide the information necessary for the models as described in Section 2.3. The output of the hysteresis block for parameters relating only to the distortion of the bladders is given in Fig. 2b and for parameters relating to pure coulomb friction in Fig. 2d.

The inertial load is a pure double integrator with output arm inertia as a denominator constant. Normally, distributed noise is injected into the feedback paths to simulate the noise measured by the experimental system transducers.

3.2 Model validation

A series of experiments were conducted to make direct comparisons between the model and experimental system performance. Except where stated, all simulation results include ±2 per cent hysteresis due to bladder distortion as illustrated in Fig. 2b. In Fig. 4 a series of three comparisons was made for the proportional-to-error controller with gains (K_e) only, with no applied friction. Figure 4a shows the simulation and Fig. 4b the experimental results obtained with a 1.7 kg m^2 payload (I) and K_e set to 1.2 V/rad. Figures 4c and 4d give the result for the same payload but with an increased proportional to error gain, $K_e = 3.7$ V/rad. In Figs 4e and 4f the payload has been decreased to 0.4 kg m^2, $K_e = 3.7$ V/rad. In all three cases there is good correlation between simulation and experiment.

The performance of a proportional-to-error controller, $K_e = 3.7$ V/rad, with ±8 per cent coulomb friction applied with the brake and a payload of 1.7 kg m^2 is illustrated in Figs 5a and 5b. In Figs 5c and 5d the payload is reduced to

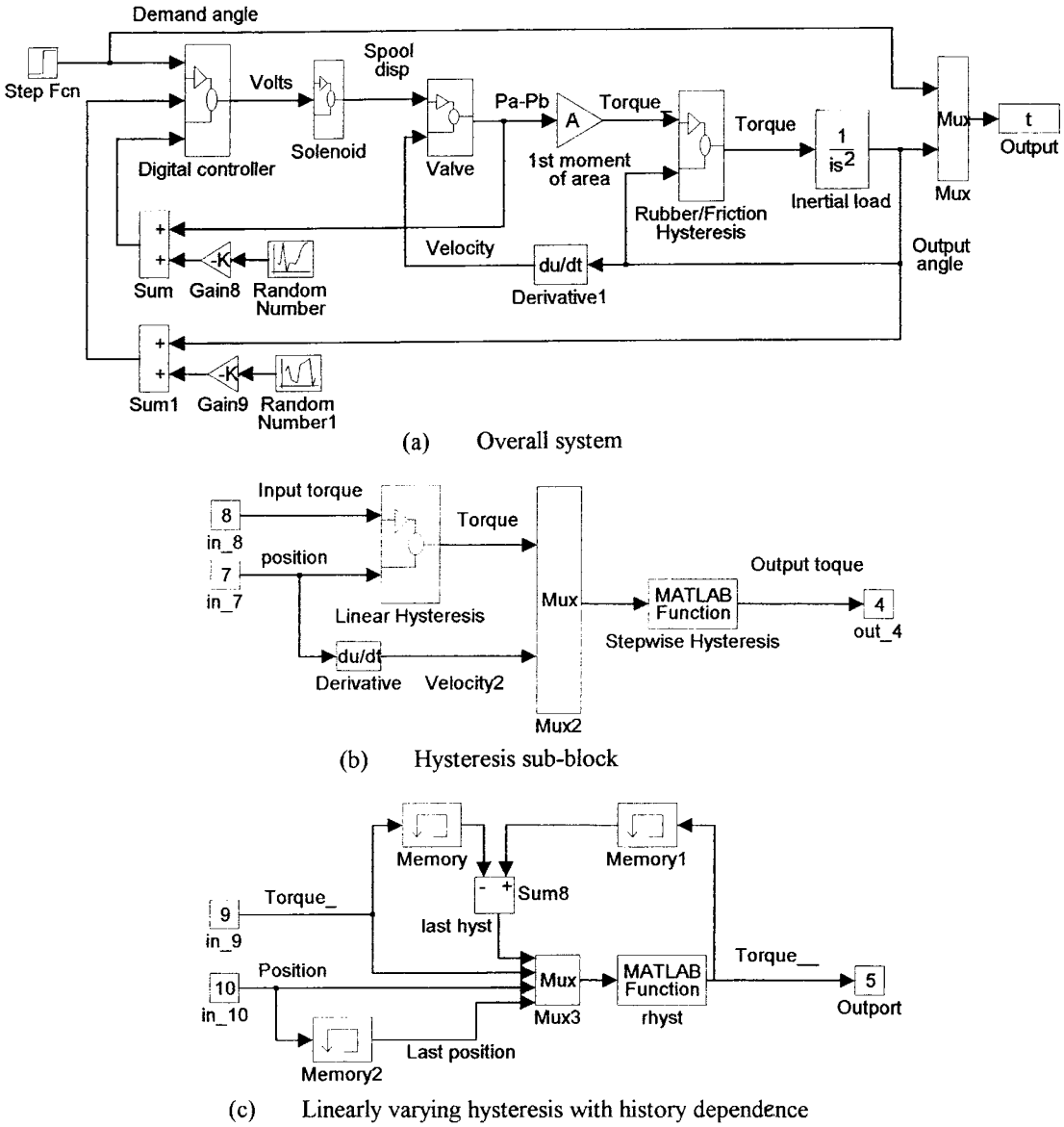

Fig. 3 SIMULINK block diagram representation

0.4 kg m^2 and the gain increased to 7.4 V/rad. In both cases the correlation between simulation and experiment is good, though not as good as the previous three runs, indicating that the coulomb friction model provides a reasonable but not perfect representation of the physical system. As expected, the coulomb friction provides a degree of damping, reducing oscillations around the set point. However, this damping has been provided at the expense of significantly increased steady state errors. In the experimental system steady state error is variable between runs but values lie in a restricted band. The experimental results given in Figs 5b and 5d are typical, but in general steady state errors are lower than those predicted in simulation. Some of the discrepancy, up to 0.007 rad, may be due to unmodelled elastic flexing of the brake assembly, which will tend to distort in such a way as to reduce error.

The use of velocity feedback is illustrated in Fig. 6. System parameters were as follows: $I = 1.7$ kg m^2, $K_e = 3.7$ V/rad, no applied friction and a velocity feedback gain of 0.3 V/rad s. The results, which display reasonable agreement between simulation and experiment, show that velocity damping has only a limited value in damping the system.

Differential pressure feedback is used in the last response illustrated in Fig. 7, where $I = 1.7$ kg m^2, $K_e = 4.9$ V/rad, $K_p = 1.7$ V/bar and no friction has been applied. Both simulation and experiment gave similar initial rates of response and steady state errors. However, the experimental result is less damped, probably due to overestimation of differential pressure within the simulation. This trait can be seen in all results (Figs 4 to 7). Differential pressure is related to the second differential term of the simulation position output and is therefore likely to highlight any

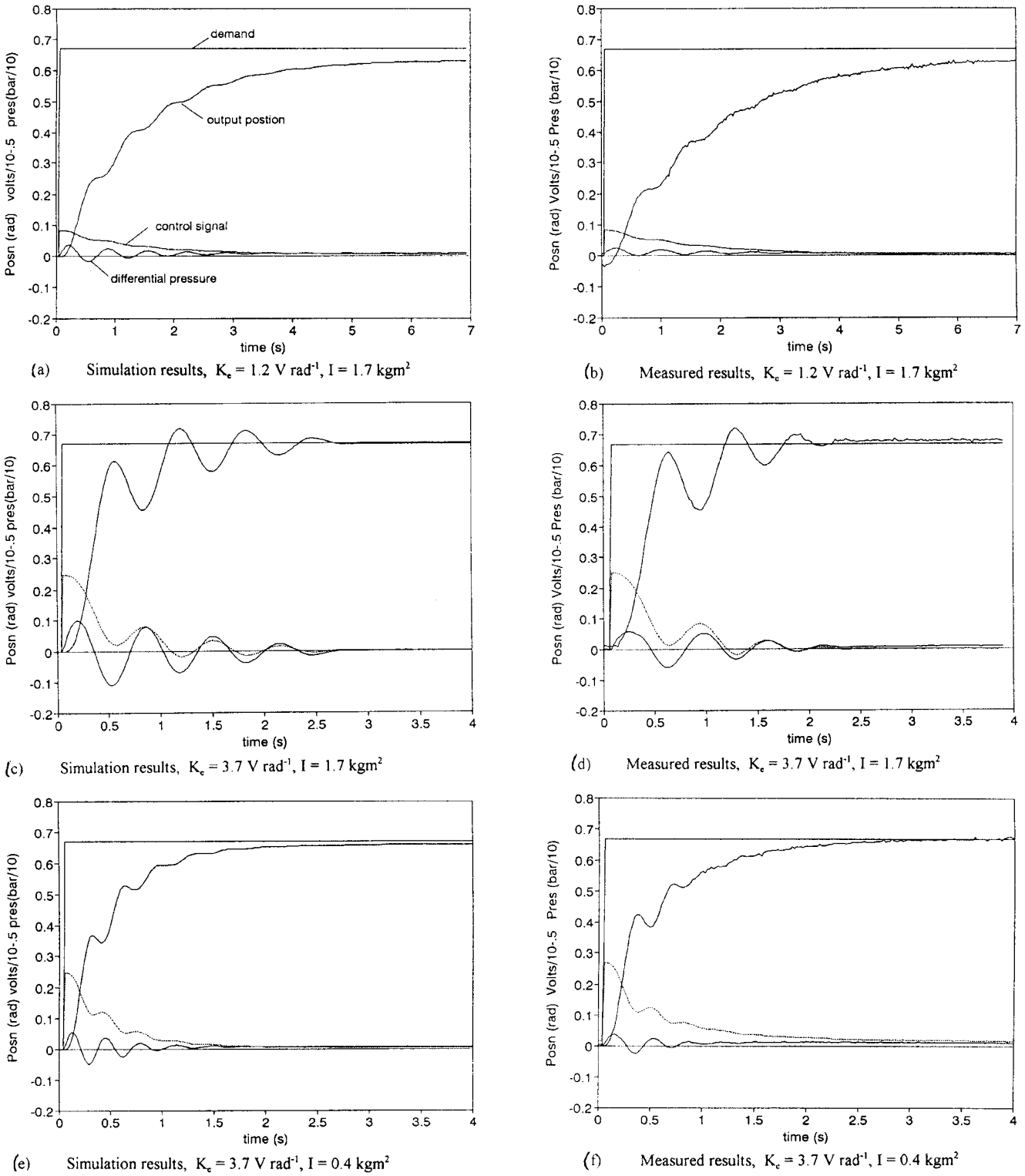

Fig. 4 Comparison between simulation and experimental results with no brake applied and a proportional to error controller

differences between real and simulated behaviour. Prediction of pressures would also seem to be the least accurate aspect (approximately ±20 per cent) of Backé and Eschmann's (**5**) simulation, though they give few results and do not comment directly on it. The effectiveness of differential pressure as a damping term is clear from Fig. 7. However, a steady state position error is caused as the controller strives to bring differential pressure to zero in the presence of hysteresis. The situation could be worse in the case of a rotary actuator if, due to manufacturing defects for

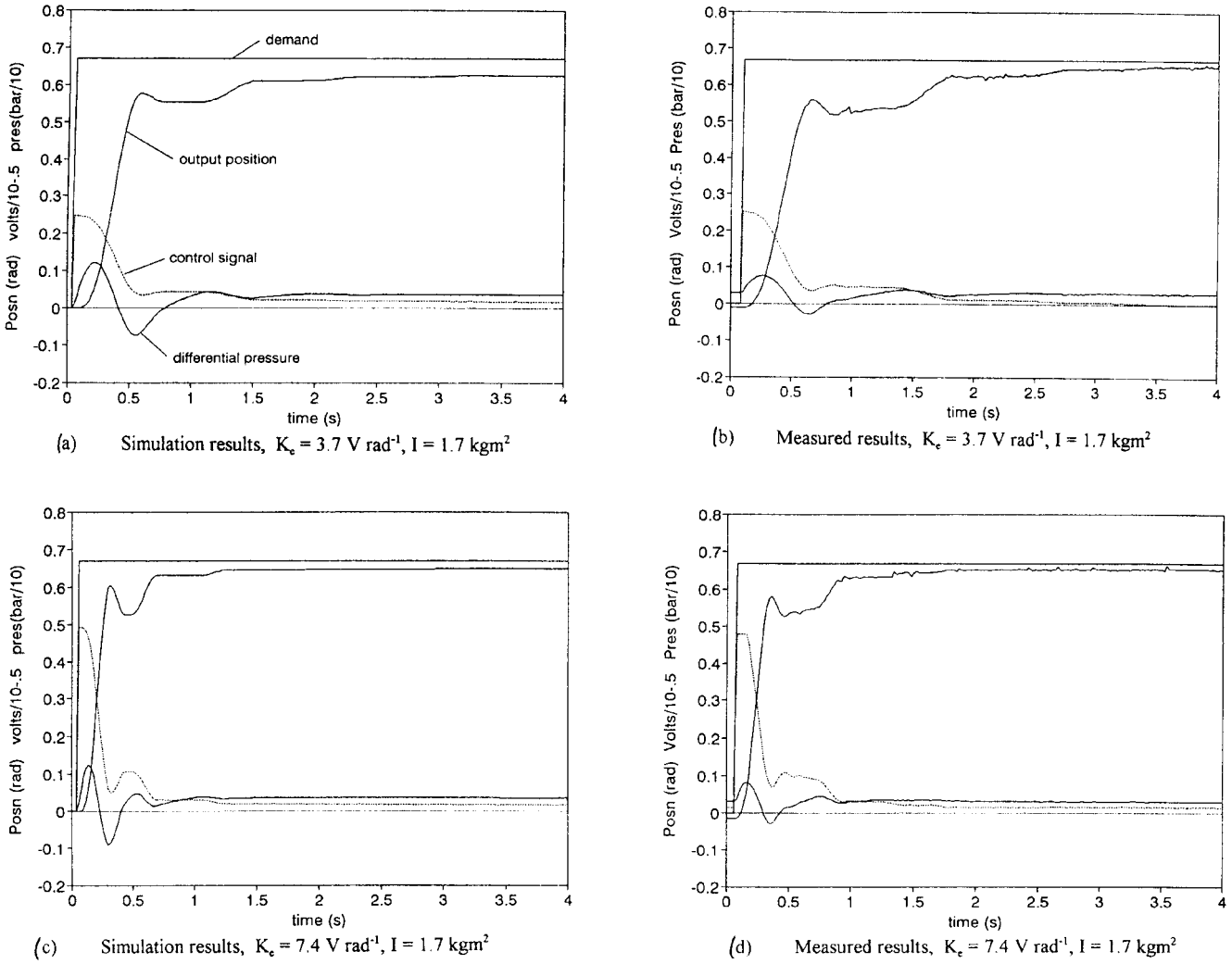

Fig. 5 Comparison between simulation and experimental results with ±8 per cent coulomb friction applied through the brake and a proportional to error controller

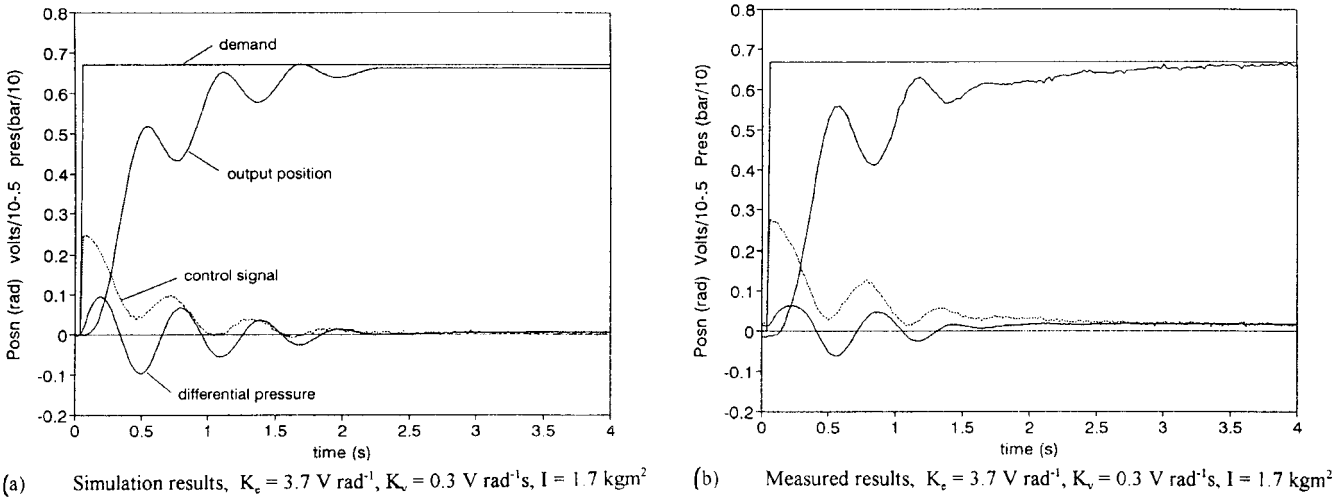

Fig. 6 Comparison between simulation and experimental results with a velocity damping term included in a proportional to error controller, no brake applied

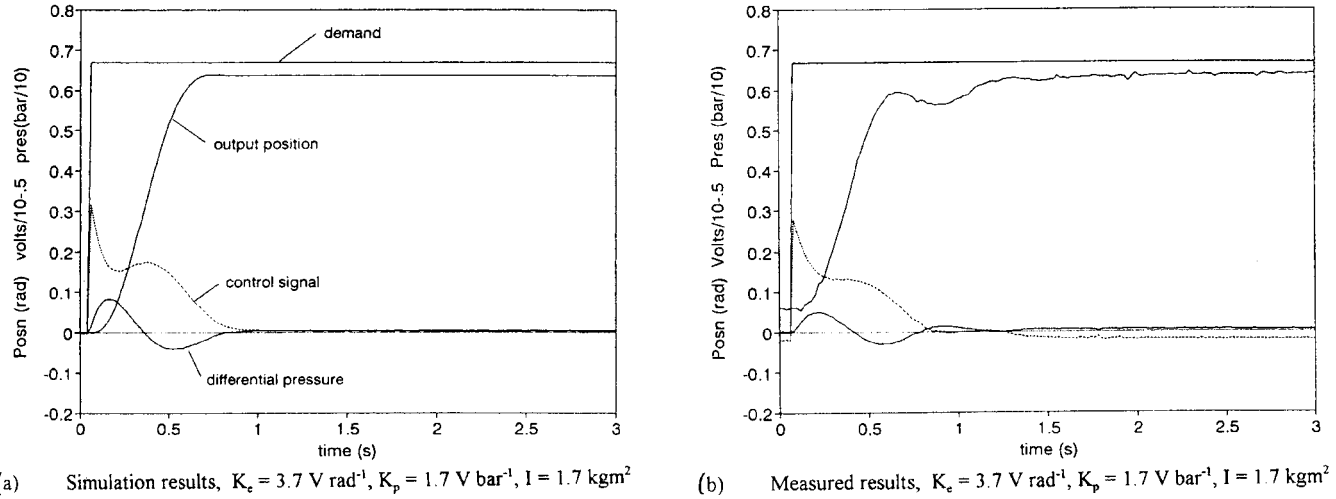

Fig. 7 Comparison between simulation and experimental results with a pressure differential between bladders damping term included in a proportional to error controller, no brake applied

example, the cam profile does not produce a perfectly constant output torque throughout its stroke. In such a case the steady state differential pressure will vary slightly with position. A solution developed by Shearer (**7**) and others is to use transient pressure feedback which will go to zero at the steady state. In 1956 Shearer proposed a method to achieve this pneumatically, though it would now be most conveniently implemented electrically or as a digital filter. A preliminary investigation of this technique applied to the rotary actuator has been conducted in simulation.

3.3 Investigations in simulation

Transient pressure feedback was implemented in simulation as a continuous transfer function of the form:

$$\frac{\tau_f s}{1+\tau_f s} \tag{18}$$

acting as a high-pass filter and placed between the analogue-to-digital converter and the point at which noise is injected. Best results were obtained with a time constant $\tau_f = 1$ s, which can be expressed as a 1 Hz cut-off frequency at the -3 dB breakpoint. The results given in Fig. 8 relate to the same parameters used to obtain Fig. 7 except that the pressure gain K_{tp} has been altered to act on the transient pressure and retains the value 1.7 V/bar. The figure shows a very marginally less damped response, but with a significant reduction in steady state error. The apparent effectiveness of this technique in simulation suggests that it might be worth implementing on the experimental system for further evaluation. An alternative, or complementary, solution to the problem of providing adequate damping, while maintaining a fast response rate and low steady state errors, may lie in using one of the many non-linear control strategies that have been proposed for pneumatic systems (**1**–**3**). The use of such strategies

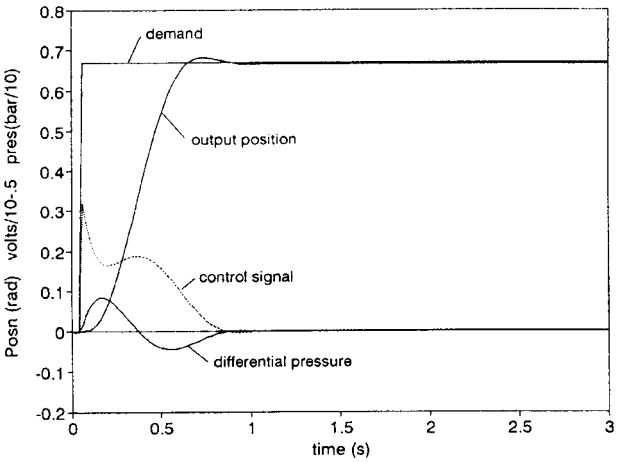

Fig. 8 Simulation result showing the effect of transient pressure feedback in a proportional to error controller, no brake applied; $K_e = 4.9$ V/rad, $K_{tp} = 1.7$ V/bar, $I = 1.7$ kg m^2

has not been investigated here, but could form the basis of future work with the simulation model.

The significance of the magnitude and type of hysteresis are investigated in the remaining figures. For reference in Fig. 9, all parameters are identical to those used to obtain Fig. 4c except that hysteresis has been eliminated. The marked change in response indicates the importance of including hysteresis within the model and shows that hysteresis contributes to system damping. It should be noted that the apparent stabilizing effect of hysteresis relates to its presence within position control systems in which oscillations around the set point result in a change in direction of movement which hysteresis opposes, thus removing energy from the system. In trajectory-following applications oscillations will result in varying speeds about the desired level but the direction of motion may remain

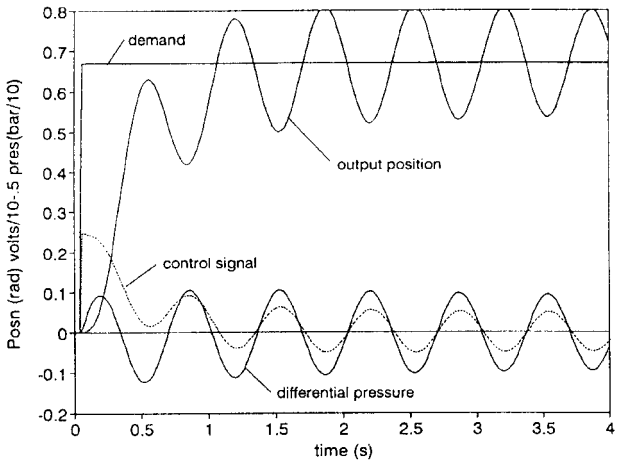

Fig. 9 Simulation result showing the effect of removing hysteresis from the model when all other parameters are the same as those used to obtain Fig. 4c; $K_e = 3.7$ V/rad, $I = 1.7$ kg m^2

unchanged and so there will be no damping effect. In both cases hysteresis will result in increased steady state errors. This effect has been demonstrated in Fig. 10 in which the addition of ± 10 per cent of coulomb friction has failed to affect the oscillations about the ramped input, though it has increased steady state error. Viersma (**11**) discusses a similar result for hydraulic servo systems and concludes that coulomb friction does not improve stability, though he only considers a constant speed input. In general, hysteresis has adverse effects on the performance of trajectory or velocity control systems, but the picture is less clear-cut for position control. This is particularly true for pneumatic systems, which can be easier to stabilize about a stationary set point with some hysteresis present. If hysteresis has some desirable features, it would be interesting to know which forms should be minimized and which, under some circumstances, might be deliberately introduced. In Fig. 11 hysteresis of the type introduced by distortion of the bladders (i.e. as represented by Fig. 2b) is compared with that due to pure coulomb friction (i.e. as represented by Fig. 2d). To exaggerate the differences hysteresis levels are ± 6 per cent in both cases. Other parameters are the same as those used to obtain Fig. 4c. The results indicate that coulomb friction induced hysteresis provides more damping than that caused by distortion of the bladders. Steady state errors are the same in both cases, indicating that it would be preferable to design-out hysteresis due to the distortion of bladders and replace it if required with pure coulomb friction.

4 CONCLUSIONS

The simulation model successfully predicts all major modes of behaviour. It provides an accurate representation of the position response of the experimental system under proportional to error or proportional to error and velocity

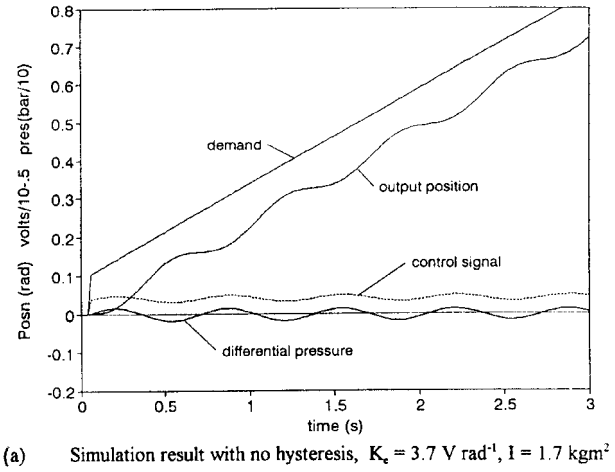

(a) Simulation result with no hysteresis, $K_e = 3.7$ V rad^{-1}, I = 1.7 kgm^2

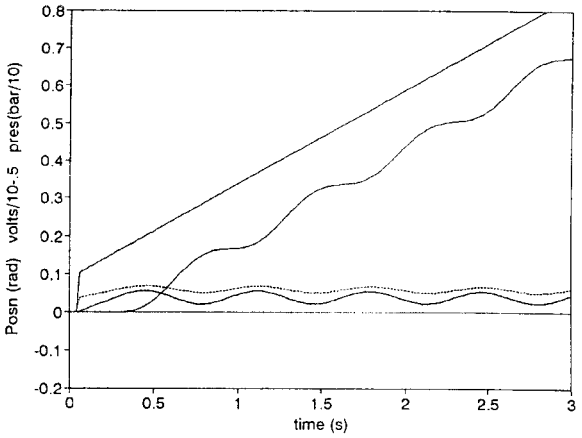

(b) Simulation result with +/- 10% Coulomb friction induced hysteresis, $K_e = 3.7$ V rad^{-1}, I = 1.7 kgm^2

Fig. 10 Investigation in simulation of the effect of coulomb friction on a proportional to error control system with a ramp input

feedback control. The simplified models of rubber and coulomb friction-induced hysteresis modify simulation performance in line with experimental results.

In general differential pressures predicted in simulation are up to 60 per cent greater than those measured in the experimental system. This discrepancy causes the damping effect of pressure feedback terms to be overestimated in simulation. The model provides a useful mechanical and control design tool for pneumatic positioning systems in general and those utilizing flexible rotary actuators in particular.

An investigation in simulation of different forms of hysteresis showed that coulomb friction-induced hysteresis had a greater damping effect than the same level of hysteresis caused by the distortion of the rubber bladders. This result applies only to position control, as hysteresis has been shown not to provide damping in trajectory control applications.

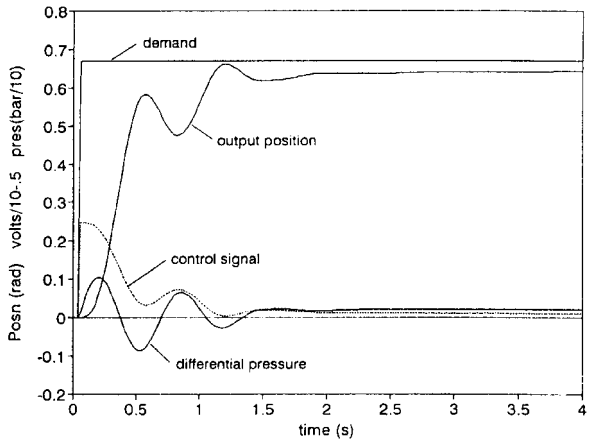

(a)

Simulation run with +/-6% hysteresis due to bladder distortion, $K_e = 3.7$ V rad^{-1}, $I = 1.7$ kgm^2

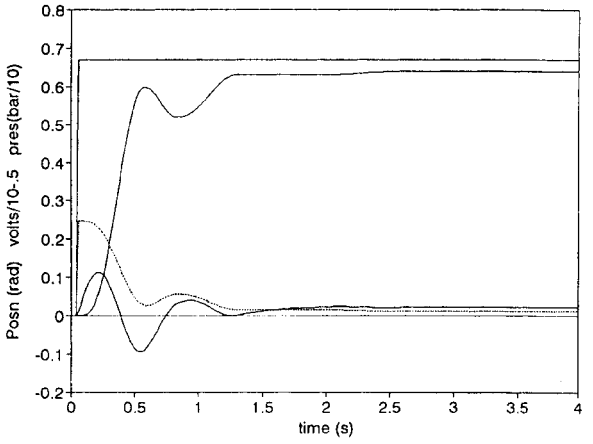

(b)

Simulation run with +/- 6% hysteresis due to Coulomb friction, $K_e = 3.7$ V rad^{-1}, $I = 1.7$ kgm^2

Fig. 11 Investigation in simulation of the differences between coulomb friction and rubber distortion-induced hysteresis in a proportional to error control system with a step input

ACKNOWLEDGEMENTS

This project has been funded by the Office of Science and Technology. The flexible actuator, registered trade name 'Flexator', has been used with the permission of Airmuscle Limited.

REFERENCES

1 **Pu, J.** and **Weston, R. H.** Motion control of pneumatic drives. *Microprocessors Microsystems*, 1988, **12**, 373–382.
2 **Belforte, G., Raparelli, T.** and **Verardocchai, M.** Fuzzy logic application to a pneumatic positioning system. *Autom. Strum. (Italy)*, April 1993, **41**(4), 95–100.
3 **Surgenor, B. W., Vaughan, N. D.** and **Uebing, M.** Continuous sliding mode control of a pneumatic positioning system. In Eighth Bath International Fluid Power Workshop, September 1995.
4 **Tillett, N. D., Vaughan, N. D.** and **Bowyer, A.** An improved flexible pneumatic joint for horticultural robots. *Mechatronics*, 1994, **4**(7), 653–671.
5 **Backé, W.** and **Eschmann, R.** SSP—a simulation program for pneumatics. In Sixth Bath International Fluid Power Workshop, September 1993, pp. 64–77.
6 **Liu, S.** and **Bobrow, J. E.** Analysis of a pneumatic servo system and its application to a computer-controlled robot. *Trans. ASME*, 1988, **110**, 228–235.
7 **Shearer, J. L.** Study of pneumatic processes in the continuous control of motion with compressed air. *Trans. ASME*, 1956, 233–249.
8 **Burrows, C. R.** Effect of position on the stability of pneumatic servo mechanisms. *J. Mech. Engng Sci.*, 1969, **11**, 615–616.
9 **Chou, C.** and **Hannaford, B.** Measurement and modelling of McKibben pneumatic artificial muscles. *IEEE Trans. Robotics and Automn*, February 1996, **12**(1).
10 *SIMULINK Users Guide*, April 1993 (The MathWorks, Inc.).
11 **Viersma, T. J.** *Analysis, Synthesis and Design of Hydraulic Servosystems and Pipelines*, 1980 (Elsevier Scientific Publishing Company, Oxford).